J Electroceram (2012) 28:45–52
DOI 10.1007/s10832-011-9676-1

Ultrasonic-assisted hydrothermal deposition of ferroelectric $PbZrO_3$ thin film on NiTi-based superelastic shape memory alloys

Florian Schiedeck · Takeshi Morita

Received: 17 December 2010 / Accepted: 4 December 2011 / Published online: 17 December 2011

Abstract The deposition of a single-layer piezoelectric thin film on superelastic shape memory alloys has been experimentally investigated. Therefore, the ultrasonic-assisted hydrothermal method was used for preparing a crystalline thin film on various NiTi-based substrates without an additional buffer layer between substrate and thin film. The deposited layers were crystallographically characterized by scanning electron microscopy, X-ray diffraction, and piezoresponse force microscopy. Due to the hydrothermal synthesis with ultrasonic assistance, the $PbZrO_3$ thin film—in general antiferroelectric—exhibits ferroelectric hysteresis loops, which has been experimentally tested.

Keywords Hydrothermal synthesis · $PbZrO_3$ thin film · Ferroelectricity · Superelasticity · Shape memory alloy

F. Schiedeck (✉)
Institute of Dynamics and Vibration Research,
Gottfried Wilhelm Leibniz Universität Hannover,
Appelstr. 11, 30167 Hannover, Germany
e-mail: schiedeck@ids.uni-hannover.de

T. Morita
Environmental Information and Microsystems Laboratory,
Department of Human and Engineered Environmental Studies, Graduate School of Frontier Sciences,
University of Tokyo, 5-1-5 Kashiwanoha,
Kashiwa-shi, 277-8563, Japan
e-mail: morita@k.u-tokyo.ac.jp

1 Introduction

Shape memory alloys (SMA) exhibit two inherent thermo-mechanical effects: pseudoplasticity and superelasticity [11, 25]. The most common alloys are based on NiTi. In almost all cases, SMA are used in (quasi)-static or low frequency (<10 Hz) applications. On the other side, piezoelectric materials are predominantly used for high frequency and ultrasonic applications. Only few researches have been carried out on the integration of SMA and piezoelectric materials in order to combine the respective benefits of both functional materials.

The flexible ultrasonic wire waveguide in [13, 14] combines a superelastic SMA wire with a piezoelectric driven ultrasonic transducer. It is assumed that the superelastic SMA remains in its austenitic phase during ultrasonic transmission and exhibits linear elastic response. Rather, the superelasticity is used in [30] for prestressing piezoelectric actuators in order to improve the stroke. In both cases, the high flexibility of a superelastic SMA is used in combination with a piezoelectric transducer, which is not really an integration of the specific properties of both material types in our understanding.

The synthesis of $PbTiO_3$ on a NiTi substrate is conducted by a two-step process [19]: first, a transitional film by an in-situ hydrothermal method and, second, an outer film on the transitional film by a sol-gel method. The focus of this work is on the preparation of a piezoelectric thin film on NiTi. A full integration of the thermal shape memory effect and piezoelectricity is used for a multifunctional wire: a thermally activated SMA wire is coated by a PZT thin film using the hydrothermal deposition method [27]. The piezoelectric

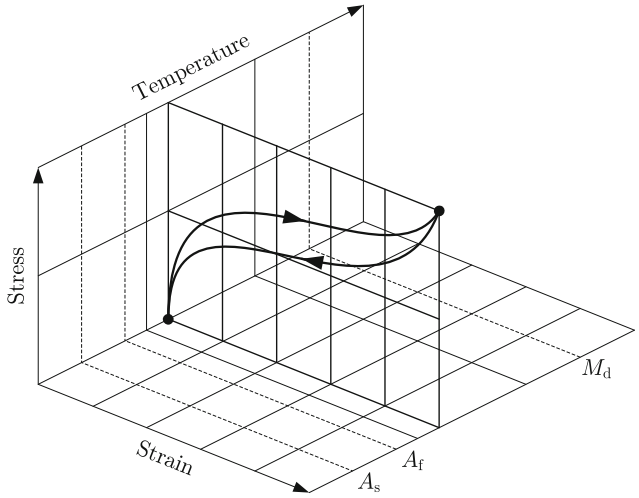

Fig. 1 Stress-strain-temperature diagram of superelasticity, where the SMA is deformed at constant temperature [29]

thin film is used for sensation rather than for excitation of the current-heated SMA wire.

Our approach pursues the concept of deposition of a piezoelectric thin film on superelastic SMA by hydrothermal method. In opposition to [27, 31], our solution contains no titanium tetrachloride $TiCl_4$ because significant health hazards generally arise from the release of hydrogen chloride HCl. Rather, titanium dioxide TiO_2, (also known as titanium(IV) oxide or titania), which is easier to handle, is preferred for preparation of a solution in combination with lead nitrate $Pb(NO_3)_2$, zirconium oxychloride octahydrate $ZrCl_2O \cdot 8\,H_2O$, and potassium hydroxide KOH [10, 16].

2 Superelastic shape memory alloys

The shape memory effect is based on a reversible martensitic transformation which can be induced by temperature (thermal shape memory effect) and mechanical stress (superelasticity) [3, 17]. The phase transformation between martensite and austenite occurs in a certain temperature interval. The start and finish temperatures of the transformation in the particular directions are defined by the transformation temperatures M_f, M_s, A_s, and A_f. Mechanical load increases the transformation temperatures directly proportional to the applied stress [35].

If the material temperature is above the transformation temperature A_f and below the desist temperature M_d, SMA exhibit the so-called superelasticity. This describes an isothermal load cycle (Fig. 1): The unloaded SMA is in austenitic phase. An increasing load deforms the SMA, and martensitic phase transformation is induced by mechanical stress. Unloading leads to a re-transformation to austenite, and the SMA returns to its original shape. The stress-strain diagram shows a distinctive hysteresis with two stress-plateaus during loading and unloading. The alternative term 'pseudoelasticity' expresses the energy dissipation as a result of the stress-strain hysteresis, where the stress-plateau during unloading is significantly smaller than during loading. Therefore, the mechanical energy for deforming is not fully released after unloading [29].

Various samples of superelastic SMA have been used as substrate for the experiments. Details about the commercial available samples are listed in Table 1. All samples are based on Nickel and Titanium (NiTi) with varying surface finish options and heat treatment conditions. Figure 2 shows different stages of processing.

The shape a SMA remembers can be set by a thermally-induced process that occurs when the SMA is constrained into its new shape and heated to temperatures of approx. 400. . . 500°C for 5 to 30 min [15, 33, 36]. The shape setting methods, e. g. types of furnaces and fixtures, are various [32]. In order to straighten the Alloy N ribbon (as drawn) and Alloy S wire (cold worked) in a preliminary treatment before hydrothermal deposition, the samples were clamped in a vise. The fixture was put into the hot furnace (450°C) with an air atmosphere and heated for 20 min. After the heat treatment, the fixture with the SMA was quenched in water.

3 Ultrasonic-assisted hydrothermal deposition

Hydrothermal synthesis is a common method for the deposition of PZT thin films. Also the deposition of PZ ($PbZrO_3$) is possible [21]. The main features are low

Table 1 Superelastic SMA samples with variable length l used as substrate for hydrothermal deposition (t: thickness, w: width, d: diameter)

Alloy	Supplier	Surface	Condition	Shape	Dimension [mm]
Alloy S	Memory-Metalle	Oxide-free (pickled)	Cold worked	Wire	$d = \varnothing\, 2.692$
Alloy S	Memory-Metalle	Oxide-free (pickled)	Flat annealed	Sheet	$t \times w = 2.0 \times 20$
Alloy N	Memory-Metalle	Dark oxide	As drawn	Ribbon	$t \times w = 0.55 \times 4.45$
Ni55/Ti45	GoodFellow	Pickled	Annealed	Foil	$t \times w = 0.5 \times 10$

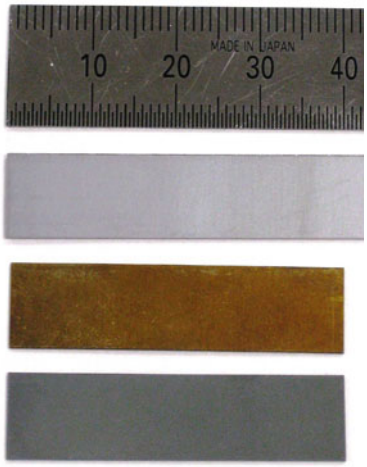

Fig. 2 Photography of Ni55/Ti45 sheets at various process stages (from *top* to *bottom* below the rule: pickled as-delivered from supplier; changed surface color with minor annealing spots after annealing process; coated with thin film by hydrothermal synthesis)

reaction temperatures below the Curie temperature, no need for post-treatment (polarization or annealing), and deposition on arbitrary shaped three-dimensional substrates. The ultrasonic-assisted hydrothermal deposition of piezoelectric thin film is performed using a ultrasonic transducer integrated in an autoclave [1, 5, 18]. Direct irradiation of ultrasound during hydrothermal synthesis improves the fabrication of fine particles.

3.1 Crystal structure

Lead zirconate titanate $Pb(Zr_xTi_{1-x})O_3$, where $0 < x < 1$, also called PZT, is a solid solution of antiferroelectric PZ ($PbZrO_3$, see below) and ferroelectric PT ($PbTiO_3$). In general, the crystals of PZT have perovskite structure. Above the Curie temperature, PZT is paraelectric. Below the Curie temperature and depending on the Zr-Ti ratio, the cubic crystal structure becomes distorted, leading to ferroelectric-tetragonal (Ti-rich) or antiferroelectric-orthorhombic and ferroelectric-rhombohedral (Zr-rich) crystals. Because the direction of the spontaneous polarization can be aligned (e. g. by applying an electric field), PZT is ferroelectric and, therefore, exhibits piezoelectricity. In absence of titanium ($x = 1$), PZT becomes PZ with orthorhombic crystal structure. In general, the ions of PZ are antiparallel and PZ is antiferroelectric. As a result, the spontaneous polarization of PZ is zero and PZ exhibits no piezoelectricity [4, 28].

However, self-aligned polarization of PZT and PZ thin films was observed when deposited by hydrothermal method and the polarization is inherently aligned in the direction of growth [20, 22, 23]. The reason for self-aligned polarization during hydrothermal deposition is not clarified yet, but might be related to the low reaction temperatures (less than Curie temperatures) and self-accumulated deposition mechanisms. It has to be proved, if the polarization direction of PZ will be also aligned when depositing with hydrothermal method. If this is the case, PZ is inherently ferroelectric and, therefore, piezoelectric.

Table 2 Solutions for ultrasonic-assisted hydrothermal synthesis of piezoelectric thin films

	Sol. A	Sol. B	Sol. C
$Pb(NO_3)_2$	7.728 g	2.070 g	2.898 g
Ti_2O	—	0.100 g	0.140 g
$ZrCl_2O \cdot 8\,H_2O$	3.652 g	0.604 g	0.846 g
KOH (8N)	40.0 ml	5.611 g	17.5 ml
H_2O	30.0 ml	50.0 ml	52.5 ml

3.2 Process conditions

The SMA samples were cleaned in an ultrasonic bath before and after hydrothermal synthesis. Following solvents were used: acetic acid CH_3COOH, acetone $(CH_3)_2CO$, ethanol C_2H_5OH, and distilled water H_2O.

For hydrothermal synthesis, various solutions (Table 2) were prepared in an autoclave including a teflon pressure vessel (inner diameter approx. ∅ 40 mm). First, powder of lead nitrate, titanium dioxide, and zirconium oxychloride octahydrate were mixed with distilled water. In a second step, a fluid solution of potassium hydroxide was added. The NiTi-based superelastic SMA were used as substrate and put into the autoclave which was approximately half-filled with the prepared solution.

The reaction time was 48 h at a constant temperature of 150°C. The ultrasonic transducer was resonantly driven with a 350 V_{pp} sine wave (300...400 mA_{pp}) at 30 kHz. The best results were obtained with solution A. Further experiments with the same substrates but varying solutions (B and C) resulted in much less homogeneous thin films. Therefore, all following experiments have been performed with solution A.

4 Crystallographic characterization

After hydrothermal synthesis, the thin film deposited on the various samples have been experimentally investigated by scanning electron microscopy, X-ray diffraction, and piezoresponse force microscopy.

4.1 Scanning electron microscopy (SEM)

The SEM was performed using a JOEL Ltd.'s JSM-5310LV. In general, all samples show a homogeneous coverage of the hole surface by a thin film. Hydrothermal synthesis without ultrasonic assistance produced less good coverage. Obviously, a preliminary heat treatment (annealing with or without shape setting) of the SMA samples improves slightly the coverage. Defects are unavoidable if samples are in contact when hydrothermally treated at the same time in one vessel. Additionally, small holes in the thin film with diameters in the range of a couple of 10 μm can appear when depositing on large substrates with lateral dimensions larger than several millimeter.

The SEM photographs of various samples in Fig. 3 show slight differences regarding cubic shape and size of crystals. The crystals deposited on an Alloy S sheet and a Ni55/Ti45 foil (both pickled) have a sharp cubic shape with an edge length of up to 5 μm. The crystals on an Alloy N ribbon (dark oxide) are more frayed but larger. The thin film thickness is measured by a scanning electron microscopy image of the polished cross-sectional area. All thin films contact well with the various substrates. The thin films deposited on an Alloy S sheet and a Ni55/Ti45 foil (both pickled) has an average thickness of 5 μm. In case of the Alloy N ribbon (dark oxide), a thin film with a thickness of up to 10 μm is deposited on a 100 μm thick oxide layer. A XRD analysis was conducted for further investigations.

4.2 X-ray diffraction (XRD)

The crystallographic structure of thin films can be characterized by XRD. The X-rays passes through the crystals and are bent at various angles, the so-called diffraction. High intensity reflection occurs at certain

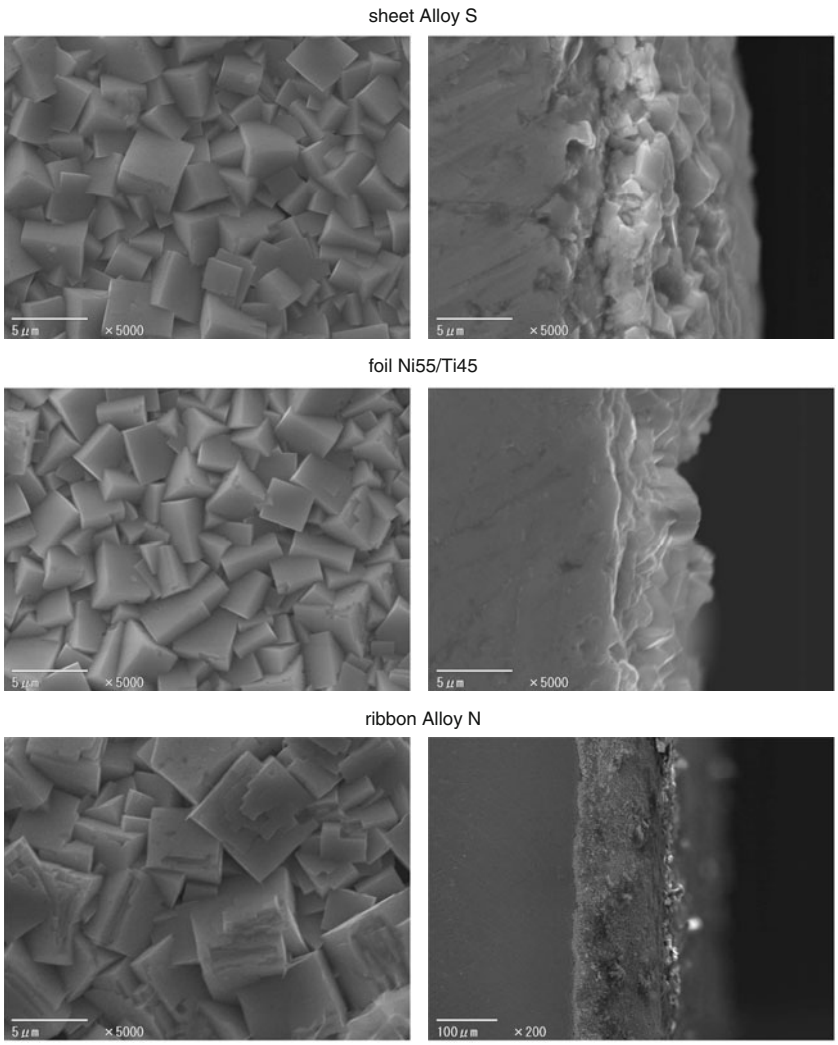

Fig. 3 SEM images of topology (*left*) and cross-sectional area (*right*) of thin films deposited on various substrates

Table 3 Lattice parameters of orthorhombic $PbZrO_3$ (space group C^8_{2v} – Pba2) [9]

Parameter	Length [Å]
a	5.8883
b	11.7581
c	8.2222

incident angles (Bragg angles) when the beams interfere constructively. The relationship for scattering angles

$$n\lambda = 2d\sin(\theta) \tag{1}$$

is called Bragg's law, where n is an integer, λ is the wave length of the incident X-ray beam, d is the distance between atomic layers in a crystal, and θ is the angle of incidence. The X-ray wavelength results from the emitted radiation of an electron transition to a lower energy level, and $\lambda = K_{\alpha 1} = 1.5405$ Å for the used copper anodes (Cu). For orthorhombic crystals

$$\frac{1}{d^2} = \frac{h^2}{a^2} + \frac{k^2}{b^2} + \frac{l^2}{c^2}, \tag{2}$$

where h, k, and l represent the Miller indices and a, b, and c are the lattice parameters. The lattice parameters for PZ are listed in Table 3.

The XRD analysis were carried out using a Mini-Flex II unit from Rigaku Corp. The results of the thin film deposited on various substrates are illustrated in Fig. 4. In addition, the calculated Bragg angles of PZ with high intensity as stated in [4, 12] are added. The closeness of agreement between experiment and calculation indicates a PZ thin film on the oxide-free substrates (Alloy S and Ni55/Ti45). The XRD of the blank substrates shows at $2\theta \approx 42.5°$ a clear peak of the austenitic NiTi(110) with cubic structure (B2 type, $a = 3.007$ Å [26]) which corresponds with the PZ(240) peak.

The XRD pattern of an Alloy N substrate (dark oxide) shows a strong congruence with the thin film deposited after nucleation in [31], where a hydrothermal synthesis with a similar solution was conducted depositing a thin film of PZ plus PZT. The authors state that even the used solution did not include any Ti, the titanium oxide layer of the substrate reacts with the solution containing lead and zirconium to build PZ and PZT crystals on the surface. In contrast, the thin film on Alloy N shows the same peaks as the oxide-

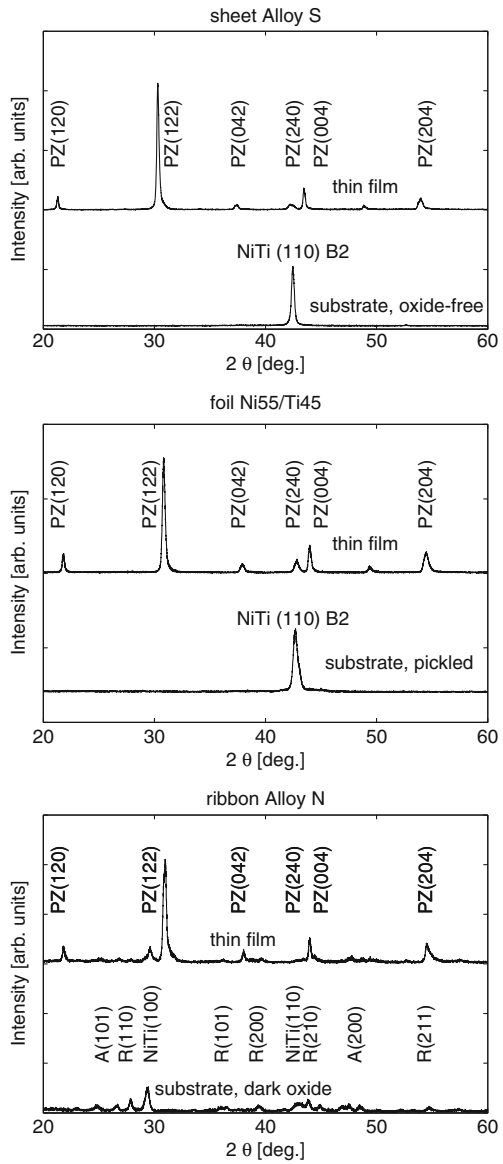

Fig. 4 XRD pattern of various substrates with thin films

Table 4 Lattice parameters of tetragonal TiO_2: rutile at 30°C and anatase at 28°C [7, 8]

Parameter	Length [Å]	
	Rutile	Anatase
a	4.5941	3.7845
c	2.9589	9.5143

Table 5 Parameter settings of PFM analysis (LiA: lock-in amplifier)

Parameter	Setting
Sweep frequency	0.30 Hz
Sweep range [μm]	10 × 10
Peak amplitude of sinusodial reference signal	10 V
Frequency of sinusodial reference signal	5 kHz
Low-pass filter time constant of LiA	1 ms
Sensitivity of LiA	10 mV

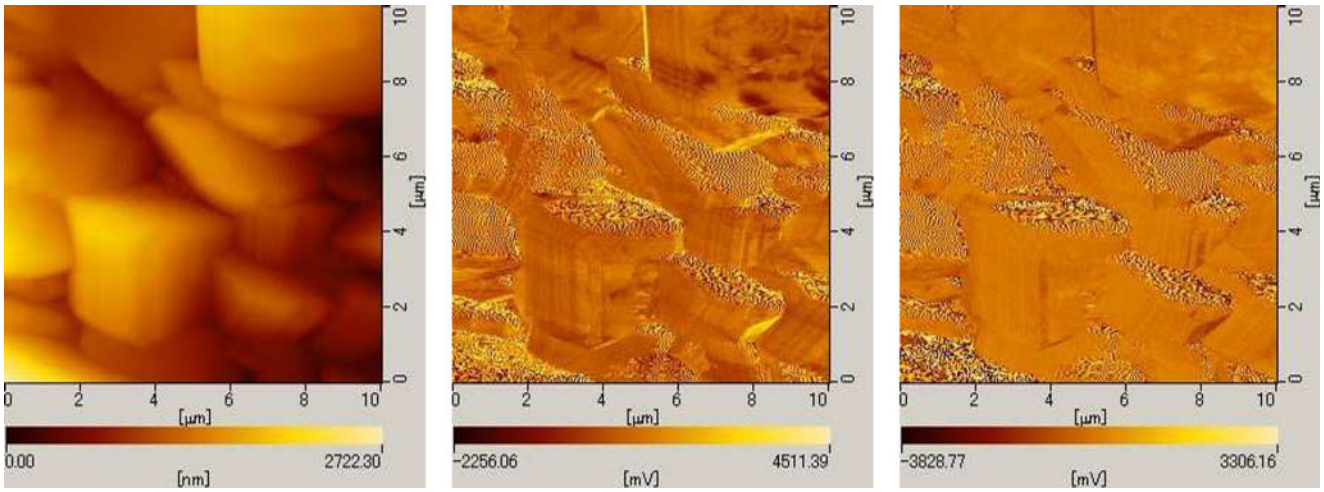

Fig. 5 PFM scan of PZ thin film on Alloy S (*left*: topology; *center*: $A\cos\phi$; *right*: $A\sin\phi$)

free samples and, therefore, is assumed to be pure PZ. An additional peak at $2\theta \approx 29°$ indicates the austenitic NiTi(100). The XRD of the blank substrate with dark oxide surface shows peaks of titanium dioxide TiO_2 crystallized in the modifications rutile (R) and anatase (A) [6, 34]. The accepted lattice parameters for TiO_2 are listed in Table 4.

A pre-treatment of the SMA samples by heating (annealing with or without shape setting, see Section 2) does not change the XRD pattern of the deposited crystals.

4.3 Piezoresponse force microscopy (PFM)

The PFM is a modification of the atomic force microscopy (AFM) for the measurement of local properties of ferroelectric and piezoelectric materials [2]. Therefore, the silicon tip is replaced by a conductive tip and an AC voltage is applied between the tip and a electrode on the opposite side of the specimen. The PFM was performed using a NanoNavi IIs (probe station) and Nanocute (general-purpose small unit) from SII NanoTechnology Inc. In addition, a FG-281 15 MHz waveform generator from Kenwood and a 5610B lock-in amplifier from NF were used. The overall settings are listed in Table 5.

The topography as well as the demodulator outputs of the lock-in amplifier, $A\cos\phi$ and $A\sin\phi$, respectively, are shown in Fig. 5. While $A\cos\phi$ represents the intensity of polarization, $A\sin\phi$ is an index for damping. The domain structure of the PZ thin film is visible in the $A\cos\phi$ measurement, and the regions of differing piezoresponse on the surface of the PZ thin film imply ferroelectricity [24]. This supports the assumption of self-aligned polarization of PZ crystals when a thin film is hydrothermally deposited (see Section 3.1).

5 Ferroelectric hysteresis

In order to prove the assumption that the PZ thin film is ferroelectric instead of antiferroelectric, the dependence of the polarization on the applied electric field was measured.

Two alternate electrodes are required for electric excitation of the thin film: the SMA substrate as inner electrode and an outer electrode on the thin film. Therefore, the electric field is applied in the direction of growth. Gold electrodes were sputtered with approx. 5 mA ion current on the thin film using a Quick Coater SG-701 from Sanyu Electron Co., Ltd. A long sputtering time or large area can cause an electric short-circuit between the inner and outer electrodes. For our investigations, a sputtering time of 5 to 10 min and a sputtering area of approx. 3.5 mm^2 were feasible.

The hysteresis measurements were carried out on a Precision LC testing unit (material analyzer and high voltage interface) from Radiant Technologies, Inc. in combination with a NF AC/DC amplifier HVA4321. The measured hysteresis in Fig. 6 confirm that a PZ thin film synthesized by hydrothermal method is ferroelectric. The PZ thin film on an Alloy S sheet and a Ni55/Ti45 foil show similar shaped hysteresis curves. The break-through voltage of the PZ thin film on the Alloy S substrate was 120 V (approx. 24 kV/mm).

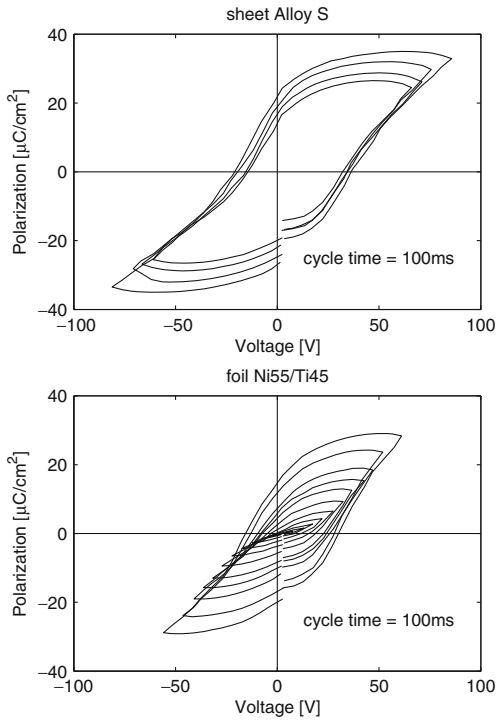

Fig. 6 Ferroelectric hysteresis loops of thin film on various substrates under different voltages

The remanent polarization $2P_r$ and coercive electric field reach more than 40 μC/cm^2 and nearly 6 kV/mm, respectively.

6 Conclusion and discussion

The deposition of piezoelectric thin films by the ultrasonic-assisted hydrothermal method on superelastic, NiTi-based SMA has been carried out, followed by a crystallographic characterization of the tin films by SEM, XRD, and PFM. A suitable solution including lead nitrate, zirconium oxychloride octahydrate, and potassium hydroxide have been identified. With it, a 5 μm thick PZ thin film has been successfully deposited on various substrates. Measurements of the polarization hysteresis has shown that the PZ thin film is ferroelectric instead of antiferroelectric.

The anomalous PZT ferroelectricity is related to the hydrothermal deposition mechanism. In previous studies, PZT [23] and PT [20] epitaxial thin films were deposited with the hydrothermal method, and their polarizations were perfectly self-aligned during the deposition process. This self-aligned polarization came from the low reaction temperature below the Curie temperature. According to these results, the present polycrystalline PZ thin films might have as well the aligned polarization; in other words, they show ferroelectricity instead of antiferroelectricity.

Another reason for ferroelectricity of ultrasonic-assisted hydrothermal deposited PZ thin films might be contamination, because the ultrasonic transducer could be slightly melted into the solution. The chemical components measurement of the PZ thin film is ongoing research. First results indicate that even if there were some contaminations inside the film, these values are negligible; therefore, contamination cannot be a conclusive reason for ferroelectricity of the deposited PZ thin film.

Acknowledgements Dr. F. Schiedeck wants to thank the Graduate School of Frontier Sciences of the University of Tokyo for the invitation and financial support as visiting assistant professor. Special thanks go to Mr R. Ageba, Mr Y. Kadota, Mr T. Maeda, and Mr K. Inoue for their assistance with the hydrothermal method and experimental characterization of PZT thin films.

References

1. R. Ageba, Y. Kadota, T. Maeda, N. Takiguchi, T. Morita, M. Ishikawa, P. Bornmann, T. Hemsel, Ultrasonically assisted hydrothermal method for ferroelectric material synthesis. J. Korean Phys. Soc. **57**(4), 918–923 (2010)
2. M. Alexe (ed.), *Nanoscale Characterisation of Ferroelectric Materials – Scanning Probe Microscopy Approach* (Springer, Berlin, 2004)
3. K. Bhattacharya, in *Microstructure of Martensite*. Why it forms and how it gives Rise to the Shape-Memory Effect. No. 2 in Oxford Series on Material Modelling (Oxford University Press, New York, 2003)
4. K. Boldyreva, Wachstum und Struktur-Eigenschafts-Beziehungen von epitaktischen antiferroelektrisch/ferroelektrischen oxidischen Multilagen. Ph.D. thesis, Martin-Luther-Universität Halle-Wittenberg (2008)
5. P. Bornmann, T. Hemsel, W. Littmann, R. Ageba, Y. Kadota, T. Morita, Ultrasonic transducer for the hydrothermal method. J. Korean Phys. Soc. **57**(4), 1122–1126 (2010)
6. V.G. Chuprina, I.M. Shalya, Reactions of tini with oxygen. Powder Metall. Met. Ceram. **41**, 85–89 (2002)
7. Collaboration: Authors and editors of the volumes III/17G-41D, in *Titanium Oxide (TiO2): Crystal Structure, Lattice Parameters and Related Parameters of Anatase*, eds. by O. Madelung, U. Rössler, M. Schulz. Landolt-Börnstein – Group III Condensed Matter, *SpringerMaterials – The Landolt-Börnstein Database*, vol 41D (Springer 2000)
8. Collaboration: Authors and editors of the volumes III/17G-41D, in *Titanium Oxide (TiO2): Crystal Structure, Lattice Parameters and Related Parameters of Rutile*, eds. by O. Madelung, U. Rössler, M. Schulz Landolt-Börnstein – Group III Condensed Matter, *SpringerMaterials – The Landolt-Börnstein Database*, vol 41D (Springer 2000)
9. Collaboration: Authors and editors of the volumes III/17H-17I-41E, in *PbZrO3 Crystal Structure, Lattice Parameters*, eds. by O. Madelung, U. Rössler, M. Schulz Landolt-Börnstein – Group III Condensed Matter, *SpringerMaterials – The Landolt-Börnstein Database*, vol 41E (Springer 2000)

10. Y. Deng, L. Liu, Y. Cheng, C.W. Nan, S.J. Zhao, Hydrothermal synthesis and characterization of nanocrystalline PZT powders. Mater. Lett. **57**(11), 1675–1678 (2003)
11. T. Duerig, K. Melton, D. Stöckel, C. Wayman (eds.), *Engineering Aspects of Shape Memory Alloys* (Butterworth-Heinemann, London, 1990)
12. H. Fujishita, S. Katano, Temperature dependence of order parameters in the antiferroelectric phase of $PbZrO_3$. Ferroelectrics **237**(1), 209–216 (2000)
13. G.P. Gavin, M. Hashmi, F. Dolan, G.B. McGuinness, in *An Acoustic Fluid-Structure Simulation of a Therapeutic Ultrasound Wire Waveguide Apparatus* ed. by H. Rodrigues. Int. Conf. on Computational Bioengineering (Lisbon, 2005)
14. G.P. Gavin, G.B. McGuinness, F. Dolan, M. Hashmi, Performance characteristics of a therapeutic ultrasound wire waveguide apparatus. Int. J. Mech. Sci. **49**(3), 298–305 (2007)
15. C. Grossmann, J. Frenzel, V. Sampath, T. Depka, A. Oppenkowski, C. Somsen, K. Neuking, W. Theisen, G. Eggeler, Processing and property assessment of NiTi and NiTiCu shape memory actuator springs. Mat.-wiss. u. Werkstofftech. **39**(8), 499–510 (2008)
16. S. Harada, S. Dunn, Low temperature hydrothermal routes to various PZT stoichiometries. J. Electroceram. **20**, 65–71 (2008)
17. J. Hesselbach, in *Shape Memory Actuators*, chap. 6.4 (Springer, 1999), pp. 143–160
18. Y. Kadota, M. Ishikawa, H. Hosaka, T.Morita, Ultrasonically assisted hydrothermal synthesis of polycrystalline PZT thin film on titanium substrate. IEEE Trans. Ultrason. Ferroelectr. Freq. Control **56**(1), 9–13 (2009)
19. X. Liu, C. Meng, D. Yang, F. Chen, New synthesis method to improve the properties of $PbTiO_3$ NiTi composite film. Mater. Des. **21**, 517–519 (2000)
20. T. Morita, Y. Cho, A hydrothermally deposited epitaxial lead titanate thin film on strontium ruthenium oxide bottom electrode. Appl. Phys. Lett. **85**(12), 2331–2333 (2004)
21. T. Morita, T. Kanda, Y. Yamagata, M.K. Kurosawa, T. Higuchi, Single process to deposit lead zirconate titanate (PZT) thin film by hydrothermal method. Jpn. J. Appl. Phys. **36**(5B), 2998–2999 (1997)
22. T. Morita, M. Kuribayashi Kurosawa, T. Higuchi, A cylindrical micro ultrasonic motor using PZT thin film deposited by single process hydrothermal method. IEEE Trans. Ultrason. Ferroelectr. Freq. Control **45**(5), 1178–1187 (1998)
23. T. Morita, Y. Wagatsuma, H. Morioka, H. Funakubo, N. Setter, Y. Cho, Ferroelectric property of an epitaxial lead zirconate titanate thin film deposited by a hydrothermal method. J. Mater. Res. **19**(6), 1862–1868 (2004)
24. M. Okuyama, Y. Ishibashi (eds.), in *Ferroelectric Thin Films: Basic Properties and Device Physics for Memory Applications*. Topics in Applied Physics, vol 98 (Springer, Berlin, 2005)
25. K. Otsuka, C. Wayman, (eds.), in *Shape Memory Alloys*. (Cambridge University Press, Cambridge, 1998)
26. B. Predel, in *Ni-Ti (Nickel-Titanium)* ed. by O. Madelung. Landolt-Börnstein – Group IV Physical Chemistry, *Springer-Materials – The Landolt-Börnstein Database*, vol 5I (Springer, 1998)
27. H. Sato, in *Development of Multifunctional Wire that Combines Shape-Memory Alloy to Piezo Electric Material*. SPIE Proc. Behavior and Mechanics of Multifunctional and Composite Materials, vol 6929 (San Diego, CA, 2008)
28. Sawaguchi, E.: Ferroelectricity versus antiferroelectricity in the solid solutions of $PbZrO_3$ and $PbTiO_3$. J. Phys. Soc. Jpn. **8**(5), 615–629 (1953)
29. F. Schiedeck, Entwicklung eines Modells für Formgedächtnisaktoren im geregelten dynamischen Betrieb. Ph.D. thesis, Leibniz Universität Hannover (2009)
30. F. Schiedeck, S. Mojrzisch, J. Wallaschek, Pre-stressing piezoelectric actuators by using superelastic shape memory alloys. J. Korean Phys. Soc. **57**(4), 889–891 (2010)
31. K. Shimomura, T. Tsurumi, Y. Ohba, M. Daimon, Preparation of lead zirconate titanate thin film by hydrothermal method. Jpn. J. Appl. Phys. **30**(9B), 2174–2177 (1991)
32. S. Smith, D. Hodgens, in *Shape Setting Nitinol* ed. by S. Shrivatsava. Proc. of the Materials & Processes for Medical Devices Concerence, Medical Device Materials, pp. 266–270 (2004)
33. Y. Suzuki, in *Fabrication of shape memory alloys*. ed. by K. Otsuka, C. Wayman. Shape Memory Materials, chap. 6 (Cambridge University Press, Cambridge, 1998), pp. 133–148
34. K. Thamaphat, P. Limsuwan, B. Ngotawornchai, Phase characterization of TiO_2 powder by XRD and TEM. Kasetsart J. (Nat. Sci.) **42**, 357–361 (2008)
35. H. Warlimont, L. Delaey, R.V. Krishnan, H. Tas, Thermoelasticity, pseudoelasticity and the memory effects associated with martensitic transformations. part 3: Thermodynamics and kinetics. J. Mater. Sci. **9**(9), 1545–1555 (1974)
36. M.H. Wu, Fabrication of nitinol materials and components, in *Proc. Int. Conf. on Shape Memory and Superelastic Technologies*, (China, 2001), pp. 285–292